Chinese Chemical Letters 31 (2020) 643–653

Contents lists available at ScienceDirect

Chinese Chemical Letters

journal homepage: www.elsevier.com/locate/cclet

Review

Recent progress of thin-film photovoltaics for indoor application

Nanfu Yan[a], Chaowei Zhao[a,*], Shengyong You[a], Yuefeng Zhang[a], Weiwei Li[a,b,c,*]

[a] Institute of Applied Chemistry, Jiangxi Academy of Sciences, Nanchang 330096, China
[b] State Key Laboratory of Organic-Inorganic Composites, Beijing University of Chemical Technology, Beijing 100029, China
[c] Beijing National Laboratory for Molecular Sciences, CAS Key Laboratory of Organic Solids, Institute of Chemistry, Chinese Academy of Sciences, Beijing 10090, China

ARTICLE INFO

Article history:
Received 16 July 2019
Received in revised form 10 August 2019
Accepted 15 August 2019
Available online 16 August 2019

Keywords:
Indoor photovoltaics
Dye-sensitized solar cells
Perovskites solar cells
Organic solar cells
Power conversion efficiency

ABSTRACT

Indoor photovoltaics have attracted increasing attentions owing to their great potential in supplying energy for low power devices under indoor light in our daily life. The third generation thin-film solar cells, including dye-sensitized solar cells, perovskite solar cells and organic solar cells, have made rapid progress from the aspect of materials design to photovoltaic performance. This review provides an overview on the recent advances in the development of indoor photovoltaic technologies based on the third generation solar cells. The design principles of advanced thin-film indoor photovoltaics were also summarized according to the characteristics of indoor light and the advantages of the third generation solar cells. Finally, after summarizing the current research progress, the perspective on this topic is provided.

1. Introduction

The practical solution to solving the problem of global energy crisis is to explore alternative clean energy resources [1,2]. It is well known that solar energy is an important source of renewable energy, owing to the merits of potential low-cost, abundant, renewable and especially environmentally benign. Photovoltaics (PV) or solar cells are considered to be one of the most effective devices for converting light energy into electrical energy, which have attracted worldwide attentions as a technique for light energy collection and utilization. Over the past six decades, scientists have struggled to search for efficient and low cost photovoltaic technologies which can be divided into three classes belonging to different generations [3]. The first generation is wafer-based solar cells, mainly crystalline-silicon (c-Si) solar cells. The second generation is thin film solar cells, such as III-V solar cells consisting of different inorganic thin films, such as amorphous silicon (a-Si), CdTe and $CuInGaSe_2$ (CIGS), *etc.* The third generation is usually accepted as advanced thin film solar cells, including dye-sensitized solar cells (DSSCs), perovskite solar cells (PSCs) and organic solar cells (OSCs). The c-Si solar cells occupy ~90% of the market and the thin film solar cells share the rest market. However, they suffer from different drawbacks, such as high production and post-processing cost for c-Si wafer, complex fabrication technology and proper disposal of polluting elements for thin film modules. Although the efficiency of the advanced thin film solar cells usually cannot compete with c-Si and normal thin film solar cells up to date, they hold great promise in fulfilling most concerns of the previous two generations. This is the main reason why the third generation of PV has dominated the research interests during the past decades.

DSSCs with power conversion efficiencies (PCEs) over 7% were first reported by Grätzel *et al.* [4], which was regarded as a milestone. Over the past two decades, DSSCs have gained significant progress with high PCEs over 14%, high stability and low production cost [5]. Nevertheless, with the rapid development of high-performing PSCs, the studies of DSSCs have been somehow ignored. PSC with a PCE of 3.8% was first reported in 2009 by Miyasaka and coworkers featuring advantages including the low-cost and easy fabrication processes [6]. By optimizing the fabrication process, the composition of perovskite layer and the interface structure, high PCEs over 20% in the lab could be obtained [7]. OSCs can be dated back to 1986, when Tang developed the first OSCs with two-layer configuration [8]. However, the boom of OSCs had not come until the bulk-heterojunction (BHJ) active layer was reported by Heeger and co-workers [9]. OSCs have the characteristics of solution processibility and light weight. Benefiting from the development of non-fullerene acceptors, PCEs of BHJ OSCs have

* Corresponding authors at: Institute of Applied Chemistry, Jiangxi Academy of Sciences, Nanchang 330096, China.
E-mail addresses: zhaochaowei1988@126.com (C. Zhao), liweiwei@iccas.ac.cn (W. Li).

https://doi.org/10.1016/j.cclet.2019.08.022

reached over 16% for single-junction device and over 17% for tandem-junction device [10–12]. Obviously, the third PV technology has the advantages of easily processing, light weight and low cost, *etc.*, endowing them great potential for flexible smart devices. Since thin film solar cell modules such as CIGS, has found growing market in the building industry, such as exterior wall and tiles, it should be the time to explore the application of the third PV generation technology in more practical fashion.

As the third generation solar cells commonly suffer from stability concerns, the application in mild indoor environment seems a more feasible way than that under standard outdoor sun light, compared to conventional c-Si panels. In recent years, the portable electronic devices, including flexible wearable devices and the Internet of Things (IoT), have rapidly penetrated into our daily life [13]. The powering of these electronic devices is undoubtedly a big energy issue. The third generation of photovoltaics has the great potential to fulfill the energy requirements of most indoor electronics, which make them very promising power candidates [14–16]. In this review, we will summarize the recent development of indoor photovoltaics (IPV) based on the third generation solar cells, including DSSCs, PSCs and OSCs. Different from the standard one sun light, there are obviously distinct characteristics of the spectrum wavelength and intensity for indoor light. This should result in diverse design principles on materials and device structures of IPV, which will be introduced in part II. The specific developing status of indoor DSSCs, PSCs and OSCs will be discussed in part III-V, respectively. A perspective respect to the material and device design of IPV technology will be provided in the last section.

2. Design principle for indoor photovoltaics

The indoor light is the power source of indoor photovoltaics, so it is necessary to discuss the characteristics of indoor light. Typically, the light intensity of the standard AM 1.5G is 100 mW/cm^2, while the light in normal offices is 1–3 orders of magnitude lower (0.01%–10%) [17]. There is a particular unit of lux for measuring the indoor light intensity. Most illuminance requirements of indoor conditions range from 200 lx to 1000 lx. It is worth noting that the lux value is of no relation with the light spectra range. Obviously, the spectrum of the indoor light mainly concentrates in the visible region. Nowadays, most of the indoor light sources are fluorescent lamp or LEDs, which present wavelength ranges from 400 nm to 700 nm [18–20]. The spectrum of a commercial white LED is shown in Fig. 1. As the market share of LEDs gradually increases, LEDs are expected to dominate indoor light sources in the future.

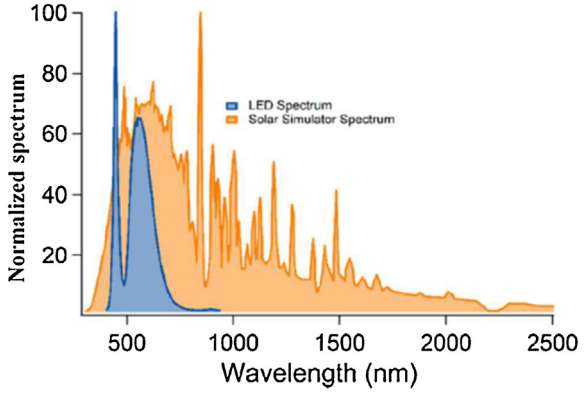

Fig. 1. The emission spectrum of a commercial white LED and an AM 1.5 G solar simulator. Reprinted with permission [18]. Copyright 2016, Royal Society of Chemistry.

For solar cell devices, efficient light harvesting is always of the paramount importance. Different from the AM 1.5G light which has wide spectra from UV–vis to infrared range, the indoor light lies in the visible range, resulting that the optimization of IPVs donot pursue the photo-active materials with narrow band gaps. Consequently, the extinction coefficient of the active layer is more important in harvesting as many photons as possible from the ambient conditions. It is proposed by Freunek *et al.* that a band gap between 1.9–2.0 eV is most appropriate for normal indoor light harvesting [21]. To improve the light absorption from the aspect of the device, more sensitizing dyes or thicker active layers can be as good candidates. Another method is to adopt the reflecting mirror layer which has been shown to enhance the overall PCEs of indoor DSSCs. As there is little UV light of the indoor environment, special UV-protective layer for standard solar cells is not necessary. The whole stability of the IPV modules can also be improved distinctly [22]. Other issues include the optimization of the interfacial layers which accounts for the charge generation and transfer. Overall, although there are arguments on the performance characterization of IPVs until now, the development of IPVs closer to commercialization should not be restrained [17].

3. Dye-sensitized solar cells for indoor application

In 1991, DSSCs with PCEs over 7% was first reported by Grätzel *et al.* [4], which was regarded as a milestone. In the past thirty years, DSSCs have gained significant progress with high PCEs over 14%, improved stability and low production cost [5]. Fig. 2 illustrates the structure of the conventional DSSC and its working principle, which were briefly described as follows: under solar illumination, dye molecules absorb photons into excited state [23,24]. The photo-generated electrons from the dyes are injected rapidly into the conduction band of TiO_2, subsequently diffuse to the FTO layer, and then pass through the external circuit to the count electrode (C). On the other hand, excited state dye molecules oxidize I^- into I_3^-, and then go back to the ground state. At the count electrode, I_3^- was reduced back to I^- through receiving electrons from the external circuit to complete the entire cycle. The I_3^-/I^- is called redox shuttle and are mainly transported through the electrolyte. Over the past few years, the DSSCs have been demonstrated to be able to perform well in ambient light and the PCEs under indoor light can be remarkably higher than those under standard one sun. The development of indoor DSSCs (i-DSSC) should be attributed to the optimization of the device units of DSSC including organic dyes, charge collecting TiO_2 and effective electrolyte forming a highly efficient collaborative system. The progress of each part will be discussed in detail respectively.

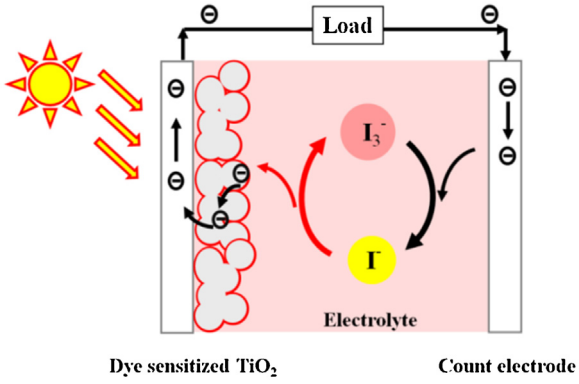

Fig. 2. Schematic diagram of DSSCs structure and working principle.

3.1. Dyes

Among the components of DSSCs, the dye sensitizers play a vital role in light harvesting, especially under low light intensity condition [25,26]. Capturing enough light is therefore crucial to improve the PCEs of the cells. The ideal dye sensitizer for DSSCs should absorb all photons of visible and near-infrared light. Table 1 provided a summary of the PCEs of DSSC based on different organic dyes under indoor light in the past few years, and the corresponding chemical structures are present in Fig. 3.

Porphyrin is well-known as the strong visible light harvesting ability, usually with high extinction coefficient. Chlorophyll is one of the most important natural dyes and can absorb sun light. Therefore, porphyrin based organic dyes should be ideal sensitizers for DSSCs. Liu *et al.* reported a simple porphyrin dye Y1A1 sensitized DSSC [27]. It was found that Y1A1-based i-DSSCs exhibited a high PCE of 19.5% under illumination intensity of 350 lx (LED light), much higher than that of 9.22% under AM1.5 G condition. Reddy *et al.* synthesized another porphyrin dye SK7 with two *N*,*N*-diarylamino moieties at two beta-positions that was used as sensitizer for DSSCs. For comparison, the photovoltaic performances of DSSC based on YD2 with one *N*,*N*-diarylamino moiety at *meso*-position was also tested. It was showed that dye YD2 based DSSC achieved the best PCE of 20.0% under illumination 6000 lx T5 light. While the DSSCs based on SK7 obtained a highest PCE of 19.7% under the same condition [28].

Anthracene based dyes represent another successful class of i-DSSC sensitizers. Wang *et al.* prepared a series of anthracene-based organic dyes (AN1, AN3, AN5, AN7, AN8) for DSSC [29]. Among them, the AN3 based DSSC module (area: 36 cm^2) achieved a PCE of 5.45% at 1000 lx (T5 fluorescent).The long-term stability of the AN-3 devices under ambient conditions was tested. The overall efficiency of the AN-3 cell dropped only 3% after 2000 h, showing the potential of AN-3 for indoor applications. Tsai and co-workers designed three other anthracene based dyes AN-11, AN-12 and AN-14 to construct i-DSSCs. The results showed that the AN-11 based i-DSSCs exhibited superior photovoltaic performance among the three organic dyes due to the panchromatic absorption of visible light. Particularly, the AN-11 based DSSC with a large active area of 26.80 cm^2 achieved an overall efficiency of 11.26% under 1000 lx (LED). As a comparison, dye Z907 based DSSC (26.80 cm^2) got a PCE of 10.91%. Moreover, it was also found that the AN-11 module exhibited good stability during the weather stress tests [30]. Tingare *et al.* demonstrated the i-DSSC based on the anthracene type dye TY6 presented the PCE of 28.56% and 20.72% under 6000 lx T5 fluorescent tube and LED light respectively. It was revealed that the absorption spectra of TY6 nicely overlapped with both blue and red regions of LED light emission. Cyclic voltammetry (CV) measurements indicated dye TY6 exhibited large energy difference between E_{LUMO} and TiO_2 conduction band which would be beneficial for electron injection. All these factors contributed to the excellent performance ofTY6 based i-DSSC [31].

Other D-A′-π-A type sensitizers were also reported. Chou *et al.* prepared push-pull organic dyes GJ-x by facile methods [32]. Photovoltaic performance of the DSSCs based on GJ-series dyes was measured under different illumination conditions. Particularly, GJ-BP dye based DSSC presentedhigh performance, with power output of 0.28 mW/cm^2 under the light intensity of 6000 lx (T5 fluorescent) which equals to PCE of 15.79%. Desta *et al.* developed four D-A′-π-A type sensitizers MD4, MD5, MD6 and MD7 with thieno[3,4-*b*] pyrazines (TP) and benzo[3,4-*b*]pyrazine (BP) as the auxiliary acceptor to fabricate i-DSSCs [33]. The MD7 based i-DSSC achieved PCEs of 18.95% and 27.17% under light intensity of 300 and 6000 lx. It was demonstrated from the electrochemical impedance spectroscopy (EIS) taken in the dark that MD7 was the best among the four dyes in suppressing dark currents owing to the twist structure, the presence of the alkoxy chains at the donor side and higher dye loading. The TKU-series were reported by Chen and co-workers [34]. The results showed that TKU-6 based DSSCs provided the best PCE of 12.21% under LED light comparing to other D-π-A structure dyes. It was also found that TKU-4 based DSSCs achieved the best PCE of13.43% under T5 lamp. This can be attributed to the match difference between the absorption of dye and the light sources. In another report by Freitag *et al.*, two dyes D35 and XY1 were combined used forming the co-sensitized DSSC. Under standard sunlight illumination, the DSSC based on D35:XY1 obtained a new record PCE of 11.3% at that time. In particular, the fabricated DSSCs also achieved high PCE of 28.9% under the indoor illumination of 1000 lx, with high external quantum efficiency (EQE) exceeding 90% among the entire visible region (400–650 nm) [35].

Table 1
The photovoltaic performance of different dyes based DSSC under low light intensities.

Dyes	E_g (eV)	J_{sc} (μA/cm^2)	V_{oc} (V)	FF	PCE (%)	P_{max} (μW/cm^2)	Light intensity (lx)	Light source	Ref.
Y1A1	1.84	52.6	0.467	0.739	19.3	18.2	300	FL	[27]
		56.6	0.476	0.755	19.5	20.3	350	LED	
SK7	1.91	739	0.584	0.778	19.7	335	6000	FL	[28]
		613	0.602	0.779	15.4	277		LED	
YD2	1.89	721	0.582	0.783	20.0	340		FL	
		626	0.604	0.785	16.5	296		LED	
AN-3	2.29	60	0.46	0.67	5.45	18.3	1000	T5 FL	[29]
		60	0.43	0.63	4.85	16.4		T8 FL	
		50	0.45	0.66	4.94	15.6		LED	
AN-11	2.0	61.5	1.05	0.643	11.94	41.6	1000	T5 FL	[30]
		52.9	1.04	0.647	11.26	35.6		LED	
TY6	2.16	883	0.717	0.785	28.56	506	6000	T5 FL	[31]
		707	0.703	0.789	20.72	394		LED	
GJ-P	2.14	594	0.597	0.74	15.01	263	6000	T5 FL	[32]
		540	0.591	0.74	13.05	237		LED	
GJ-BP	2.03	640	0.567	0.76	15.79	276		T5 FL	
		557	0.561	0.76	13.1	237		LED	
MD5	2.10	762	0.651	0.790	23.17	394	6000	T5 FL	[33]
MD7	2.01	913	0.676	0.764	27.17	462			
TKU-4	2.22	56	0.58	0.70	11.49	22.9	600	LED	[34]
		59	0.60	0.70	13.43	24.8		T5 FL	
TKU-6	2.14	61	0.56	0.71	12.21	24.3		LED	
		62	0.55	0.70	12.74	23.6		T5 FL	
XY1:D35	1.97/2.39	138	0.797	0.80	28.9	88.5	1000	FL	[35]

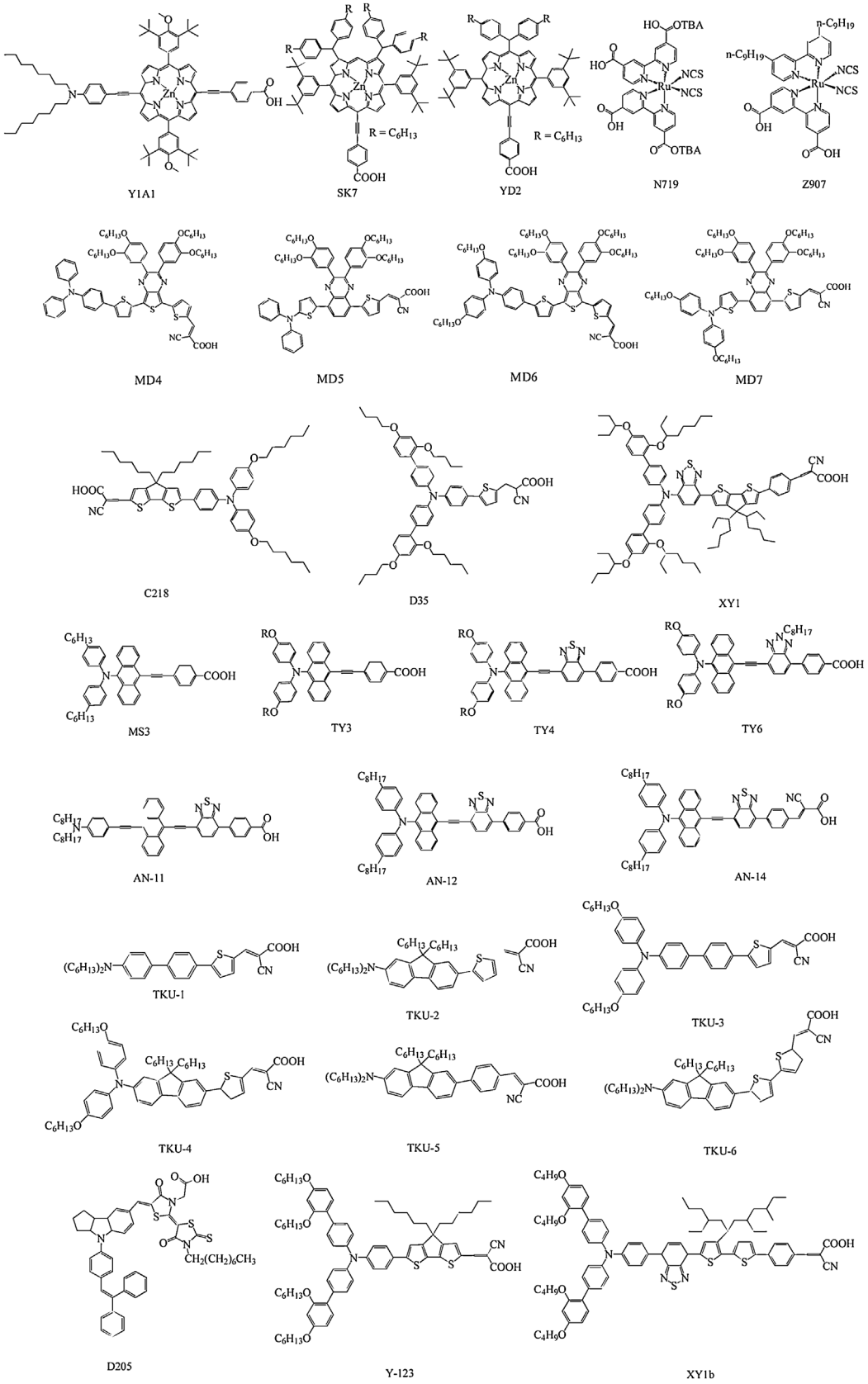

Fig. 3. Molecular structures of dyes used for indoor thin film photovoltaics based on DSSCs.

3.2. Reflecting mirror

In addition to the sensitizer selectivity, the use of reflecting mirror was another effective way to increase the absorption of light, especially under low intensities. Kapil *et al.* investigated a new type of cylindrical DSSCs based on Titanium coil (C-DSSCs) [36]. For better indoor light utilization, reflecting mirror was used to tap diffused light to further improve the photovoltaic performance of the DSSC. It was showed that N719 based C-DSSCs got a PCE of 14.95% with reflector. Huang and co-workers reported an innovative DSSC-roof hybrid configuration for indoor artificial lighting, which was constructed on the backside of the chromatic Ti foil, and Ti foil was used as working electrode. The facet-textured TiO_2 layer on the chromatic Ti foil was beneficial for improving the optical reflectance for better light utilization and suppressing the charge recombination for better electron collection. The optimal i-DSSC achieved higher efficiencies of 8.22 and 5.3% under light intensity of 1000 and 600 lx, respectively, which was improved by 42% and 31% compared to those based upon non-treated Ti under the same test condition [37].

3.3. Blocking layers

On the other hand, reducing the charge recombination is also conducive to improving the photovoltaic performance of DSSC under low light intensity. The application of blocking layers (BL) was almost the most common method to reduce the charge recombination [38]. Liu *et al.* studied the effect of the compact TiO_2 BL through different methods on the photovoltaic performance of DSSCs [39]. $TiCl_4$-derived TiO_2 on the FTO surface exhibited low surface coverage and non-uniformity. When the compact BL was prepared by spray pyrolysis on the bare FTO, the crystalline facets became gentle and the surface displayed a smoother morphology. $TiCl_4$ BL based DSSC displayed low PCEs of 8.56% and 6.19% under low light intensities of 1001 lx and 250 lx, owing to the considerable decreases in both open-circuit voltage (V_{oc}) and FF. The sprayed compact BL based DSSC obtained outstanding efficiencies 15.26% and 15.12% under the same conditions. It was revealed that the compact TiO_2 BL can inhibit electron leakage for the DSSCs more efficiently.

Zhai *et al.* prepared ultra-small and ultra-fine TiO_2 quantum dots, and successfully used TiO_2 quantum dots as a compact layer (CL) [40]. It was found that DSSCs with the TiO_2 QDs-CL achieved a high efficiency of 18.3% under illumination intensity of 7000 lx (T5 fluorescent light). It was clarified that the efficient suppression of electron recombination at the FTO/electrolyte interface by the TiO_2 QDs-CL plays significantly role in improving the photovoltaic performance. Wang *et al.* reported a DSSC using Zn-doped TiO_2 film, which can enhance the PCE by 23% under a low light intensity of 11 mW/cm^2 [41]. It was demonstrated from intensity modulated photocurrent spectroscopy and intensity modulated photovoltage spectroscopy that the difference between electron life time and transit time was large enough under low light intensities for the Zn-doping photoanode. Zn-doping can shorten the electron transit time and minimize the localization of photogenerated electrons by trap states. The charge collection efficiency of the Zn-doped film remained at considerably high levels under low light intensity, which can ensure the high performance of i-DSSCs. Chen *et al.* fabricated a DSSC using Nb_2O_5 thin film as blocking layer [42]. The blocking effect of Nb_2O_5 thin film on charge recombination under various light intensities was studied. It was demonstrated from impedance analysis and the open-circuit voltage (V_{oc}) decay examination that the Nb_2O_5 thin layer can effectively suppress the charge recombination on the photoanode. It was showed that the PCEs of DSSCs were successfully enhanced by 10% to 53% between the low light intensities of 300 lx to 6000 lx.

3.4. Electrolyte

The electrolyte of DSSC is mainly composed of polar solvent and soluble ion pair salt as the redox shuttle. The redox shuttle is crucial for completing the electrochemical circuit in both transferring electrons from the counter electrode and the dye regeneration. The choice of effective redox electrolyte has significant effect on the PCEs and stability of DSSCs.

Lan *et al.* studied the influence of iodine content on the PCEs of i-DSSCs [43]. It was demonstrated from the current-voltage behavior and EIS results that lower iodine content electrolyte offered higher PCEs at lower light intensity owing to that lower iodine content electrolyte led to relatively higher transparency and less electron recombination at the interface of photoanode and electrolyte. The conversion efficiency of DSSCs has reached a high value of 12.03% at low light intensity of 5 mW/cm^2, much higher than that of 7.28% at light intensity of 100 mW/cm^2. Small molecular transition metal complexes, such as $[Cu(dmp)_2]^{2+}$ and $[Co(bpy)_3]^{2+}$, with reduction/oxidation potential, were also demonstrated to be able to act as redox mediatorsini-DSSCs [35,39,44–46].

The liquid electrolyte always suffered from the risk of safety issues. Therefore, the purse of solid state electrolyte is highly desired and i-DSSCs based on solid electrolyte have been developed recently. Venkatesan *et al.* fabricated a *quasi*-solid-state DSSCs (QS-DSSCs) by using printable polymer gel electrolytes and they studied the effect of the composition of the electrolytes and the thickness of the photoelectrode on photovoltaic performance [47]. The results showed thatthe iodine concentration and the thickness of TiO_2 film had a great effect on PCE of the QS-DSSCs. After optimization, the QS-DSSCs obtained conversion efficiencies of 15.39% and 20.63% under low light intensities of 200 lx and 600 lx, respectively, which are comparable to that of the corresponding liquid-state DSSC. Moreover, a sub-module cell (active area 11.21 cm^2) got a relatively high PCE of 12.23% under 200 lx light. The QS-DSSC presented high stability after 1000 h testing, retaining 97% of its initial PCE. The long-term stability of the QS-DSSCs based on N719 and Z907 dyes was conducted. It showed that the N719-and Z907-based QS-DSSCs could remain 95% and 97% of the initial PCEs after 1000 h test, respectively, under light illumination of 200 lx at 35 °C under the atmosphere, indicating a high and similar stability of the QS-DSSCs using the two dyes.

3.5. Architecture

The design and optimization of the architecture of DSSC was considered to be an effective way to reduce the internal resistance and improve the photovoltaic performance of DSSC under low light intensities. Cao and co-workers constructed an advanced DSSC structure, where the photoanode and the counter electrode are directly contacted without any spacer (Fig. 4) [46]. It was demonstrated from EIS that the direct contact of the TiO_2 photoanode with the PEDOT counter electrode can reduce the diffusion path of redox mediator to merely the mesoporous TiO_2 film, resulting in the decreased Warburg resistance. The Y123/XY1b co-sensitized DSSC device gave a PCE of 13.1% under AM 1.5 G, and the corresponding PCE under light intensity of 1000 lx can be up to 32%.

4. Perovskites solar cells for indoor application

Over the past decade, PSCs have attracted worldwide attention owing to the rapidly increased PCEs as well as the low-cost and easy fabrication processes. Kim *et al.* reported an all solid-state mesoscopic heterojunction PSCs with a PCE of 9.7% [48]. By

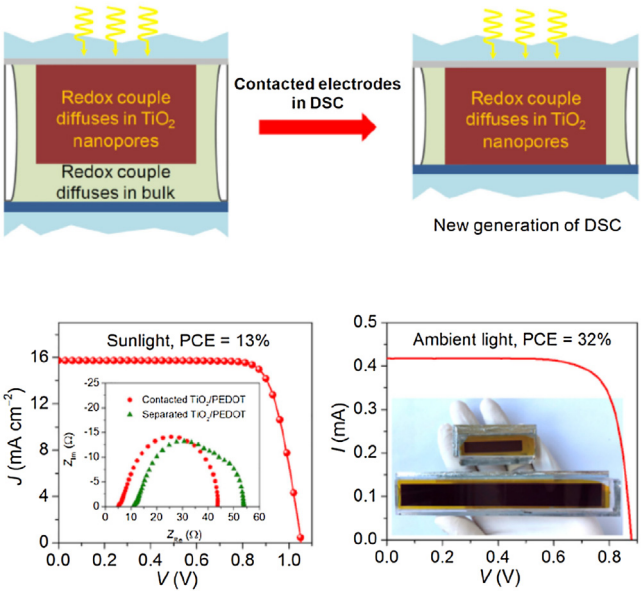

Fig. 4. Efficient energy conversion in DSSCs from artificial indoor light. Reprinted with permission [46]. Copyright 2018, Elsevier.

improving the fabrication process, and optimizing the composition of perovskite active layer and interfaces, PCE of more than 20% can be obtained in the lab [7]. The typical perovskite methylammonium lead iodide (MAPI) is of high absorption coefficient, high carrier mobilities, and low binding energy of excitons, which endows PSCs suitable for light energy harvesting and conversion. The advantages of the easy fabrication processes, and low raw material costs make perovskite photovoltaics ideal choice for indoor light harvesting to power small scale electronic devices. Generally speaking, the PSCs consist of three components, including electron transport layer (ETL), hole transporting layer (HTL), and active layer (perovskite). Fig. 5 illustrates the schematic diagram of a representative PSC structure and its working principle. As the research of indoor PSC (i-PSC) has concentrated on the (MAPI) active layer up to date, the interfaces (ETL and HTL) optimization were mainly involved to explore the i-PSC performance (Table 2) [49].

Appropriate ETL material should display suitable energy level, good optical transparency, relatively high electron mobility and environmental stability, which facilitates the electron injection from the perovskite absorber to cathode. Optimization of suitable ETL was considered to be an effective approach to improve the photovoltaic performance of PSC under low light intensities. There are mainly two kinds of PSC structures, *i.e.*, the conventional and inverted structures

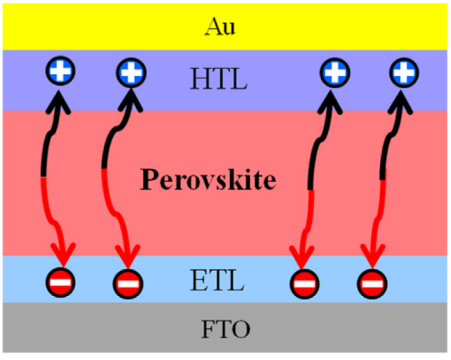

Fig. 5. Schematic diagram of a representative PSC structure and its working principle.

respectively. For Conventional PSC structures, the ETL is usually composed of a compact and a mesoscopic TiO_2 layer. Di Giacomo *et al.* reported a series of PSCs with compact TiO_2 layers through different preparation methods including spray pyrolysis technique, sol-gel process and atomic layer deposition (ALD) [50]. Especially, PSC with TiO_2 layers prepared by ALD achieved a high PCE of 24% under low light intensity of 200 lx, and 25.4% under low light intensity of 400 lx. It is notable that Lucarelli *et al.* applied the ALD derived compact TiO_2 layer on flexible PET/ITO substrate fabricating flexible i-PSCs, which gave an appreciable PCE of 12.1% under 400 lx LED light [51]. In addition to TiO_2, SnO_2 can also be used as ETL in PSCs. Dagar and co-workers studied the SnO_2-based PSCs which gave a PCE of 21.9% under 400 lx indoor LED light. It was interesting that when a thin MgO layer was introduced between SnO_2 and perovskite, the PCE could be enhanced to 26.9% under the identical condition [52]. It was demonstrated that MgO layer can lead to more uniform film and suppressed interfacial carrier recombination, which also resulted improved device stability. Moreover, in another report by Cheng *et al.*, the SnO_2 based device can be fabricated in air through an air knife-assisted recrystallization method which is quite close to industry application [53].

For the conventional structures mentioned above, Spiro is always employed as the HTL. While for inverted structures, the fullerene derivatives and even carbon materials are used as ETL and PEDOT/PSS is one of the most used HTL. Lee *et al.* investigated three types of PSCs, *i.e.*, the TiO_2/Spiro based conventional mesoporous PSC (mPSC), the PCBM/PEDOT:PSS based inverted PSC (iPSC) and TiO_2:ZrO_2:carbon based cPSC (Fig. 6) [54]. The spiro-based mPSC gave a P_{max} of 115.6 μW/cm^2 under 1000 lx LED light, while the iPSC with PEDOT:PSS only displayed a P_{max} of 77.5 μW/cm^2. When PEDOT:PSS was replaced by poly(*N*,*N*′-bis-4-butylphenyl-*N*,*N*′-bisphenyl)benzidine (poly-TPD), the power output can be increased to 111.9 μW/cm^2 which is quite comparable to that of mPSC. Notably, the HTL-free cPSC cell presented a promising P_{max} of 89.4 μW/cm^2 under light intensity of 1000 lx. It was demonstrated that the leakage current was closely related to the performance of PSC under low light intensities. With respect to the PSC for indoor application, leakage current was suggested to be controlled below 10^{-3} mA/cm^2.

Chen *et al.* demonstrated that with a thin 1,3,5-tri(*m*-pyrid-3-yl-phenyl)benzene (TmPyPB) overlayer, the $PC_{61}BM$ based inverted device presented a higher PCE about 26.3% under light intensity of 1000 lx with fluorescent lamp [55]. In particular, the large area PSC based on PCBM (5.44 cm^2) also showed a high efficiency of 20.4% under light intensity of 800 lx. Very recently, they further revealed that using C_{60}/TmPyPB and MoO_3/TPTPA as ETL and HTL respectively, the vacuum-deposited perovskite based PSC gave a high PCE up to 30.1% at 1000 lx FL condition [56]. TPTPA is tris[4-(5-phenylthiophen-2-yl)phenyl]amine. Furthermore, the long-term stability of the vacuum-deposited PSCs was also measured under low light intensities for 1 year in a normal indoor environment (temperature 20–30 °C, relative humidity 50%–70%). The encapsulated devices were placed on a shelf in office and far from windows. The results showed that the PCE of the PSCs under illumination of 600 lx only showed a small decrease of 1.3% of its peak value in 1 year with simple epoxy encapsulation without any desiccant. It suggested that the lifetimes of the PSCs operating under gentle indoor environment could be largely extended compared with that of the PSCs operating under much harsher bright one sun condition.Li and co-workers introduced 1-butyl-3-methylimidazolium tetrafluoroborate ([BMIM]BF_4) as a protective layer for constructing a planar PSC [57]. The PSC showed an impressive PCE of 35.20% at light intensity of 1000 lx. In particular, the PCE of a large area (4 cm^2) device also could also be up to 23.16% under 1000 lx light. It was demonstrated that [BMIM]BF_4 had much stronger modification effect on passivating the net positive charge

Table 2
The photovoltaic performances of PSC under various light intensities.

ETL	HTL	J_{sc} (μA/cm^2)	V_{oc} (V)	FF	PCE (%)	P_{max} (μW/cm^2)	Light intensity (lx)	Light source	Ref.
TiO_2	Spiro	58	0.775	0.72	25.4	32.6	400	FL	[50]
TiO_2	Spiro	33.7	0.662	0.77	12.1	16.0	400	LED	[51]
SnO_2	Spiro	63.3	0.873	0.61	21.9	34.0	400	LED	[52]
SnO_2/MgO	Spiro	64.5	0.895	0.72	26.9	41.6			
SnO_2	Spiro	–	–	>0.75	27.0	–	500-2000	FL	[53]
TiO_2	Spiro	173.7	0.91	0.73	–	115.6	1000	FL	[54]
PCBM	Poly-TPD	172.5	0.86	0.75	–	111.9			
TiO_2/ZrO_2/C	w/o	174.9	0.72	0.72	–	89.4			
$PC_{61}BM$/TmPyPB	PEDOT:PSS	132.3	0.84	0.75	26.3	–	1000	FL	[55]
C_{60}/TmPyPB	MoO_3/TPTPA	135	0.88	0.75	30.1	94.9	1000	FL	[56]
PCBM/[BMIM]BF_4	NiO_x	150	0.87	0.75	35.2	–	1000	FL	[57]

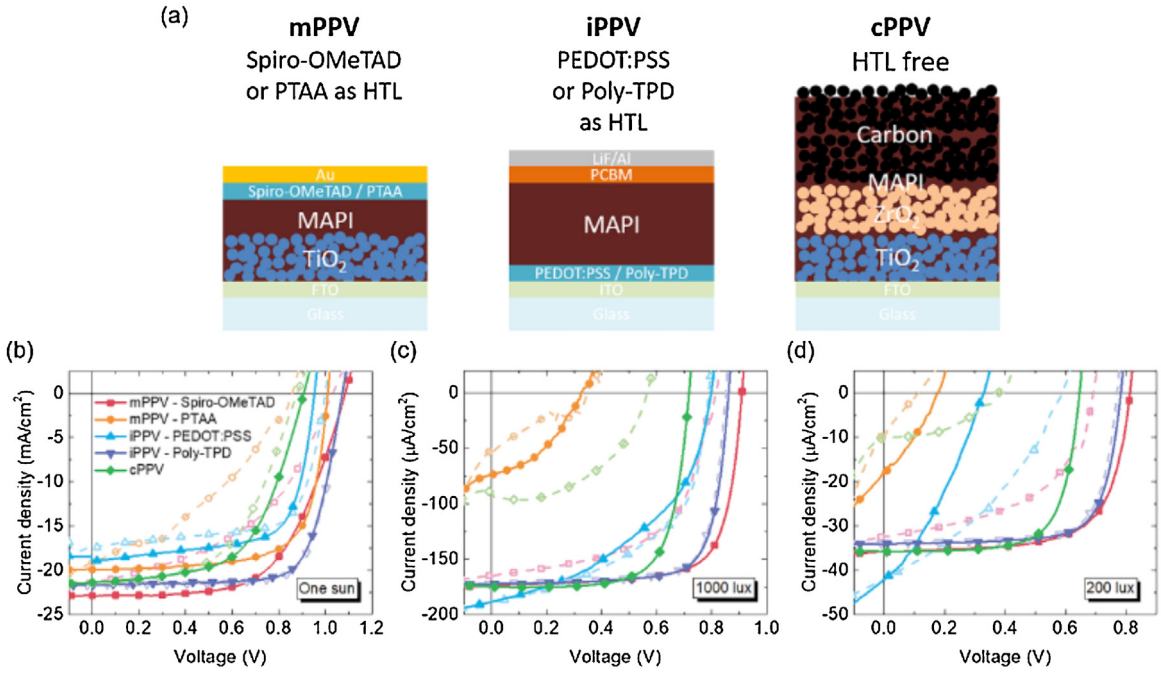

Fig. 6. (a) Schematic diagram of three types of perovskite device architectures studied in this work. *J–V* characteristics under one sun (b), fluorescent lamps of 1000 lx (c) and fluorescent lamps of 200 lx (d). Solid lines and dash lines represent reverse and forward scan of the *J–V* measurements, respectively. Reprinted with permission [54]. Copyright 2019, John Wiley and Sons.

on the perovskite surface. Furthermore, the [BMIM]BF_4 could also significantly improve the stability of PSC by restraining the moisture and oxygen infiltrating into the perovskite layer. At 80 °C, the PCE of the [BMIM]BF_4-based PSCs can keep 73% of the initial value even after 95 h storage, while the BCP-based PSCs can just keep 45% of the initial value.

5. Organic solar cellsfor indoor application

Since the BHJ structure was developed (Fig. 7), the OSCs have witnessed great progress during the past two decades [58–61]. Owing to their intrinsic advantages, such as light weight and low cost, OSCs are used to integrate with some low power supplied and even flexible electronics [62]. The relatively mild indoor conditions can endow the organic photovoltaics more close to practical application. Actually, the indoor OSCs (i-OSCs) have attracted growing research attention during the past 5 years. Compared to classical c-Si solar cells, i-OSC can display quite promising power output [18]. According to the structure of OSCs, this part will be discussed with respect to the BHJ active layer (Table 3), charge collecting interfacial layer and special device integration, such as series modules and photo-rechargeable system, respectively.

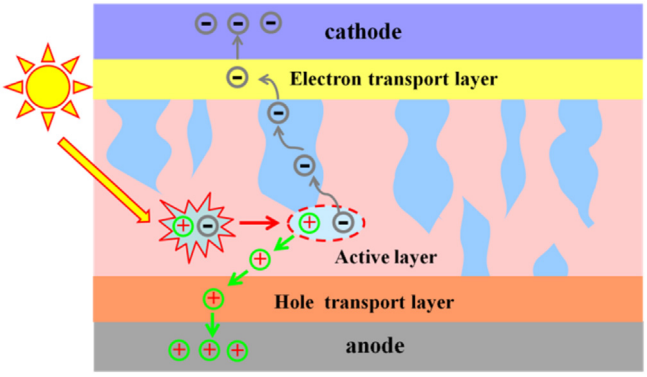

Fig. 7. Schematic diagram of OSCs structure and working principle.

5.1. Active layer

Similar to the light harvesting dyes in DSSCs, the donor/acceptor materials of BHJ layer in i-OSC should display matching absorption with the indoor light spectra (Fig. 8). The pursue of low

Table 3
Summary of representative active layers measured under different indoor light conditions.

Active layer	E_g (eV) of donor	J_{sc} (μA/cm^2)	V_{oc} (V)	FF	PCE (%)	P_{max} (μW/cm^2)	Light intensity (lx)	Light source	Ref.
P3HT:P_{61}CBM	2.1	62	0.43	0.59	9.59	15.77	500	FL	[63]
		62	0.43	0.59	8.50	15.67		LED	
P3HT:ICBA	2.1	50	0.73	0.62	13.76	22.57	500	FL	
		50	0.73	0.63	13.05	22.97		LED	
PBDTTT-EFT:PC_{71}BM	1.6	63	0.58	0.59	13.14	21.56	500	FL	
		66	0.59	0.58	13.20	23.23		LED	
PTB7-Th:PC_{71}BM	1.6	92	0.62	0.74	11.63	42.3	890	LED	[64]
P3HT: PC_{61}BM	2.1	20.6	0.41	0.57	5.8	4.8	300	FL	[65]
PCDTBT:PC_{71}BM	1.9	27.7	0.72	0.69	16.6	13.9			
PTB7:PC_{71}BM	1.8	28.6	0.61	0.70	14.6	12.2			
PDTBTBz-2F:PC_{71}BM	2.0	112.4	0.817	0.70	23.1	66	1000	LED	[66]
P3HT:PC_{71}BM	2.1	73.7	0.498	0.72	9.4	26.8			
PBDB-T:PC_{71}BM	2.0	90.2	0.669	0.71	15.3	43.7			
PTB7:PC_{71}BM	1.8	87.6	0.569	0.69	12.3	35.1			
PPDT2FBT:PC_{71}BM	1.76	117	0.587	0.65	16.0	44.8	1000	LED	[67]
PCDTBT:PDTSTPD:PC_{71}BM	1.9/1.73	33.3	0.73	0.64	20.8	15.4	300	FL	[68]
PCDTBT:PTB7:PC_{61}BM:PC_{71}BM	1.9/1.9	43.7	0.582	0.71	10.6	18	500	LED	[69]
PTB7-Th:PBDB-T:PC_{71}BM:ITIC-Th	1.6/1.8	105.1	0.662	0.66	16.3	45.65	1000	LED	[70]
		118.4	0.684	0.64	15.8	50.72		FL	
DTCPB:C_{70}	2.04	79	0.72	0.64	15.78	36.63	800	FL	[71]
BTR:PC_{71}BM	1.8	133	0.79	0.75	28.1	78.2	1000	FL	[72]
P1:PC_{71}BM	1.5	29.56	0.758	0.66	19.2	14.86	300	LED	[73]

band gap materials to harvest as many photons as possible for standard one sun illumination is not suitable to i-OSC systems. It was estimated by Freunek *et al.* that the optimum band gap for harvesting indoor LED or fluorescent light is 1.9 eV, rather than that of 1.4 eV for standard sunlight [21]. Polymer donors with wide and narrow band gaps combined with fullerene acceptors often gave comparable PCEs under indoor light conditions [63–67]. Among the polymer donors reported by now, the spectrally matched donor PDTBTBz-2F, with 2.0 eV band gap, gave the best PCE of 23.1% and 66 μW/cm^2 power output under 1000 lx LED illuminance [66]. This PCE has exceeded the best PCE of OSCs under AM 1.5 G illumination. For i-OSC devices, the J_{sc} is almost linearly correlated to the light intensity, while the V_{oc} is logarithmically dependent on the illuminance intensity. However, the relationship of FF with light intensity has not been well revealed. As with reducing the light intensity, in some cases the FF was decreased, while in other systems, the FF can be improved evidently [63,66].

Another appealing is that i-OSC active layer is more suitable for thick films. Under low light irradiation, the charge recombination is less happened without sacrificing much J_{sc} and FF. Many BHJ i-OSC devices work best with more than 200 nm active layer thickness. For PPDT2FBT:PC_{71}BM, the device gave the best PCE of 16% with 390 nm active layer, while the device with 870 nm layer retained a PCE of 12.5% under 1000 lx LED light [67]. The thick film tolerance is greatly beneficial to roll-to-roll large area module production.

The multi-component strategy has been widely adopted to improve the sunlight harvesting in BHJ OSCs to increase the PCE under AM 1.5 G irradiation and this is also applied to i-OSCs. Under 300 lx FL irradiance, the ternary PCDTBT:PDTSTPD:PC_{71}BM layer exhibited superior PCE of 20.8% exceeding the binary PCDTBT:PC_{71}BM device of 16.5% [68]. Very recently, two i-OSC systems with quaternary BHJ layers were also demonstrated. One adopted two polymers PCDTBT:PTB7 as bi-donors and two fullerene derivatives PC_{61}BM:PC_{71}BM as bi-acceptors [69]. The other was consisted of PTB7-Th:PBDB-T as bi-donors and PC_{71}BM:ITIC-Th as bi-acceptors, in which ITIC-Th belongs to the fused ring A-D-A type non-fullerene acceptors [70]. The combination of fullerene and non-fullerene acceptors in the latter can efficiently suppress the domain growth and segregation thus improve the device stability. Moreover, all small molecular i-OSCs were also paid attention in past years [71–73]. The BTR:PC_{71}BM based device gave an outstanding PCE of 28.1% under 1000 lx FL irradiation through optimization with solvent vapor annealing. This PCE is the champion for i-OSCs and quite comparable to other indoor thin film photovoltaics up to date [72].

5.2. Interfacial layer

In general, the OSC devices can be fabricated in conventional or inverted structures respectively. The conventional structures are usually ITO/PEDOT:PSS/active layer/LiF/Al or ITO/PEDOT:PSS/active layer/Ca/Al with hole transport layer PEDOT:PSS contact with conducting ITO substrate. Kyaw and co-workers investigated the influence of Ca thickness on the *p*-DTS(FBTTh$_2$)$_2$:PC_{71}BM based device performance under different light intensity. They revealed the dominance of the first-order recombination from the short-circuit site to maximum power point (MPP), which switched to bimolecular recombination from the MPP to open-circuit voltage [74].

The inverted configuration is to fabricate the electron transport layer just on ITO glass, such as ITO/PFN/active layer/Mo_xO/Ag and ITO/ZnO/active layer/Mo_xO/Ag. Goo and Vincent *et al.* demonstrated that ITO/PEIE and ITO/SiO_x/PEIE can act as electron collecting electrode in place of ZnO film under indoor light. PEIE is polymeric ethoxylatedpolyethylenimine modifying on the surface to decrease the work function (WF) [19,75]. To overcome the high cost of ITO glass, Goo and co-workers employed 200 nm thick ZnO nanoparticles on normal glass by atomic layer deposition method acting as transparent conducting electrode (TCE) [76]. The devices with structure of glass/ZnO/PEIE/P3HT:ICBA/MoO_X/Ag can hardly work under AM 1.5 G illumination, but can exhibit excellent indoor performance with a PCE of 9.5% under 500 lx LED light. The silence of the device under 1 sun condition can be attributed to the high sheet resistance of the ZnO film (260 Ω/sq), while the indoor performance is mainly related to the high shunt resistance for lower linkage current. In another report, they fabricated quasi-amorphous ZnO/Ag/ZnO TCE on flexible polyethylene terephthalate (PET) substrates. The P3HT:ICBA based device not only gave superior PCE higher than the reference ITO device under indoor LED light, but also exhibited excellent mechanical stability [77].

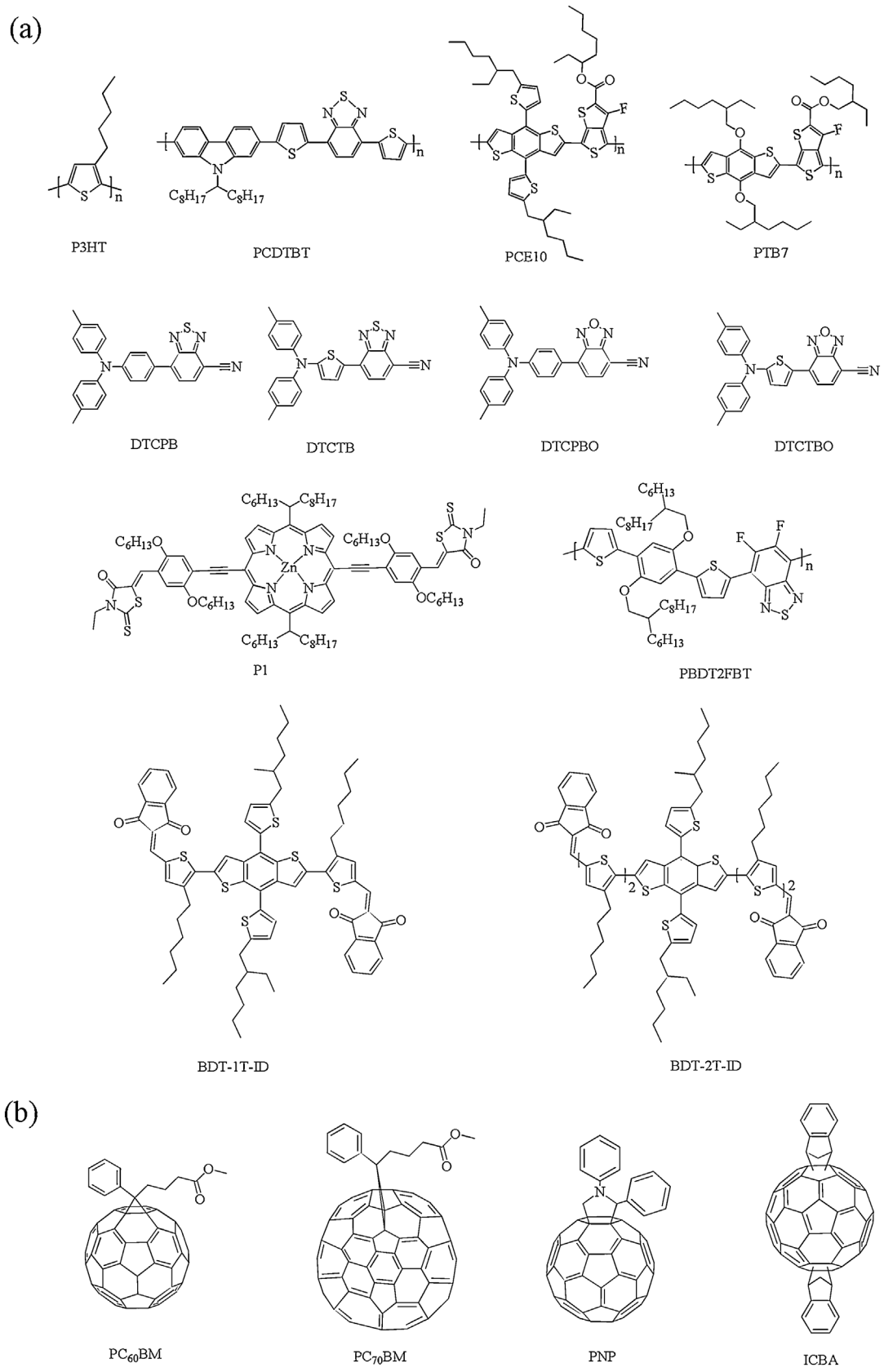

Fig. 8. Molecular structures of active layers materials used for indoor thin film photovoltaics based on OSCs. (a) Donor conjugated materials and (b) fullerene derivatives.

5.3. Special device integration

For IPVs commerciallization, the requirement for enough voltage output has to be solved. The series modules integration is an effective approach to increase the voltage and power output [78]. Arai *et al.* fabricated six series connected modules of the BDT-nTID:PNP blended OPV systems. The whole active area was up to ~10 cm^2 and the generated output power surpassed 100 μW with a high V_{oc} of over 4.2 V even under 200 lx LED conditions [79]. To realize all weather power supply, the photo-rechargeable system is a good choice. Lechêne and co-workers integrate the OPV and a fully printed super-capacitors. This combined system can realize a energy conversion and storage efficiency (ECSE) of 1.56% under one sun and 1.07% under specific indoor light conditions, corresponding to the stored energy of 26 mJ and 13.3 mJ respectively [80].

6. Summary and perspective

In summary, the basic concept of indoor thin-film photovoltaics was given and the characteristics of the different types of indoor thin-film photovoltaics based on DSSC, PSCs and OSCs were introduced. The design of indoor photovoltaics with high efficiency under the identical conditions and long-term stability was undoubtedly a challenging task. Although high efficiencies were reported for indoor thin-film photovoltaics in the laboratories all over the world, the long-term stability of the indoor thin-film photovoltaics still needs to be improved in order to adapt to domestic and commercial applications in the future.

(1) Currently, most of the research works of DSSCs, PSCs, and OSCs are measured under a standard sunlight. In reality, the different light sources are used inside various kinds of laboratories, and indoor environment illuminant condition is different as well as intensity and spectrum characteristic. Illumination conditions are not uniform for indoor thin-film photovoltaics, including the type of LED light source, light intensity, *etc.* To the best of our knowledge, there is still no test standard for measuring the characteristics of indoor thin-film photovoltaics, which needs to be established and standardized.

(2) At present, the design of solar cells with high performance for indoor application still lacks a unified theoretical research mode, which need more research works to understand the above deficiencies. Under low light intensity, the law of the characteristics change of indoor thin-film photovoltaics, such as short-circuit current, open-circuit voltage, and filling factor, need to be further clarified.

(3) Principles of materials optimization. The construction of indoor thin-film photovoltaics with high conversion efficiency and long-term stability need materials with excellent performance. When selecting materials, clear principles of optimization are needed to save time and cost. For example, as the spectrum of indoor light ranges from 400 nm to 700 nm, wide band gap materials should be selected to construct OSCs.

(4) Photovoltaics stability studies under standard solar illumination conditions have been reported a lot. However, there are few studies about the stability under indoor light conditions. Under indoor conditions, light intensity and air humidity are relatively reduced, it is believed that indoor thin-film photovoltaics will presented better stability.

(5) Indoor photovoltaic (PV) will play a major role in supplying energy to low operation power devices or low power wireless electronic devices in the future. In particular, indoor thin-film photovoltaics can integrate with electrochemical energy storage device, such as rechargeable batteries and capacitors to form photo-rechargeable systems (Fig. 9) [81,82]. On one hand, those devices can convert weak light into electrical energy under low light intensity. On the other hand, they can also store excess electrical energy inside the devices, which can output electricity in the absence of light.

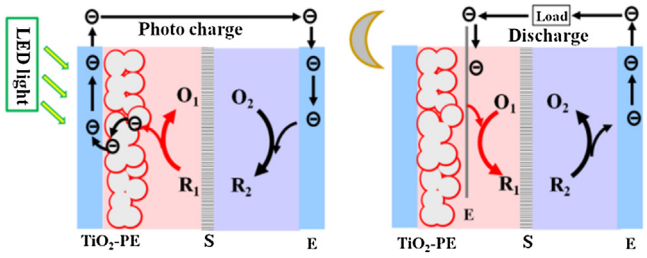

Fig. 9. Schematic diagram of solar rechargeable battery structure and working principle.

Acknowledgments

N. Yan acknowledges financial Supports from Natural Science Foundation of Jiangxi (No. 20161BBE50095). This study is jointly supported by Ministry of Science and Technology (No. 2017YFA0204702) and National Natural Science Foundation of China (No. 51773207, 21574138, 21801213). This work was further supported by the Strategic Priority Research Program of the Chinese Academy of Sciences (No. XDB12030200) and Fundamental Research Funds for the Central Universities (No. XK1802-2).

References

[1] N. Armaroli, V. Balzani, Synth. Lect. Energy Environ. Technol. Sci. Soc. 4 (2011) 3193–3222.
[2] M.S. Dresselhaus, I.L. Thomas, Nature 414 (2001) 332–337.
[3] G. Conibeer, Mater. Today 10 (2007) 42–50.
[4] B. Oregan, M. Gratzel, Nature 353 (1991) 737–740.
[5] K. Kakiage, Y. Aoyama, T. Yano, et al., Chem. Commun. (Camb.) 51 (2015) 15894–15897.
[6] A. Kojima, K. Teshima, Y. Shirai, T. Miyasaka, J. Am. Chem. Soc. 131 (2009) 6050–6051.
[7] A.K. Jena, A. Kulkarni, T. Miyasaka, Chem. Rev. 119 (2019) 3036–3103.
[8] C.W. Tang, Appl. Phys. Lett. 48 (1986) 183–185.
[9] G. Yu, J. Gao, J.C. Hummelen, F. Wudl, A.J. Heeger, Science 270 (1995) 1789–1791.
[10] G. Zhang, J. Zhao, P.C.Y. Chow, et al., Chem. Rev. 118 (2018) 3447–3507.
[11] X. Xu, K. Feng, Z. Bi, et al., Adv. Mater. (2019) 1901872.
[12] L.X. Meng, Y.M. Zhang, X.J. Wan, et al., Science 361 (2018) 1094–1098.
[13] Y. Zhan, Y. Mei, L. Zheng, J. Mater. Chem. C Mater. Opt. Electron. Devices 2 (2014) 1220–1232.
[14] F.C. Chen, Adv. Optical Mater. 7 (2019)1800662.
[15] Z.L. Wang, W. Wu, Angew. Chem. Int. Ed. 51 (2012) 11700–11721.
[16] I. Mathews, S.N. Kantareddy, T. Buonassisi, I.M. Peters, Joule 3 (2019) 1415–1426.
[17] C.Y. Chen, Z.H. Jian, S.H. Huang, et al., J. Phys. Chem. Lett. 8 (2017) 1824–1830.
[18] C.L. Cutting, M. Bag, D. Venkataraman, J. Mater. Chem. C Mater. Opt. Electron. Devices 4 (2016) 10367–10370.
[19] J.S. Goo, S.C. Shin, Y.J. You, J.W. Shim, Sol. Energy Mater. Sol. Cells 184 (2018) 31–37.
[20] B. Minnaert, P. Veelaert, Energies 7 (2014) 1500–1516.
[21] M. Freunek, M. Freunek, L.M. Reindl, IEEE J. Photovolt. 3 (2013) 59–64.
[22] H. Pettersson, T. Gruszecki, Sol. Energy Mater. Sol. Cells 70 (2001) 203–212.
[23] A. Hagfeldt, G. Boschloo, L. Sun, L. Kloo, H. Pettersson, Chem. Rev. 110 (2010) 6595–6663.
[24] J. Gong, K. Sumathy, Q. Qiao, Z. Zhou, Renew. Sustain. Energy Rev. 68 (2017) 234–246.
[25] J.M. Cole, G. Pepe, O.K. Al Bahri, C.B. Cooper, Chem. Rev. 119 (2019) 7279–7327.
[26] B. Pashaei, H. Shahroosvand, M. Graetzel, M.K. Nazeeruddin, Chem. Rev. 116 (2016) 9485–9564.
[27] Y.C. Liu, H.H. Chou, F.Y. Ho, et al., J. Mater. Chem. A: Mater. Energy Sustain. 4 (2016) 11878–11887.
[28] K.S.K. Reddy, Y.C. Liu, H.H. Chou, et al., ACS Appl. Mater. Interfaces 10 (2018) 39970–39982.
[29] C.L. Wang, P.T. Lin, Y.F. Wang, et al., J. Phys. Chem. C 119 (2015) 24282–24289.
[30] M.C. Tsai, C.L. Wang, C.W. Chang, et al., J. Mater. Chem. A: Mater. Energy Sustain. 6 (2018) 1995–2003.
[31] Y.S. Tingare, N.S.N. Vinh, H.H. Chou, et al., Adv. Energy Mater. 7 (2017) 1700032.
[32] H.H. Chou, Y.C. Liu, G. Fang, et al., ACS Appl. Mater. Interfaces 9 (2017) 37786–37796.
[33] M.B. Desta, N.S. Vinh, C.H. Pavan Kumar, et al., J. Mater. Chem. A: Mater. Energy Sustain. 6 (2018) 13778–13789.

[34] C.H. Chen, P.T. Chou, T.C. Yin, et al., Org. Electron. 59 (2018) 69–76.
[35] M. Freitag, J. Teuscher, Y. Saygili, et al., Nat. Photonics 11 (2017) 372–378.
[36] G. Kapil, Y. Ogomi, S.S. Pandey, T. Ma, S. Hayase, J. Nanosci. Nanotechnol. 16 (2016) 3183–3187.
[37] C.H. Huang, Y.W. Chen, C.M. Chen, ACS Appl. Mater. Interfaces 10 (2018) 2658–2666.
[38] B. Peng, G. Jungmann, C. Jäger, et al., Coord. Chem. Rev. 248 (2004) 1479–1489.
[39] I.P. Liu, W.H. Lin, C.M. Tseng-Shan, Y.L. Lee, ACS Appl. Mater. Interfaces 10 (2018) 38900–38905.
[40] P. Zhai, H. Lee, Y.T. Huang, et al., J. Power Sources 329 (2016) 502–509.
[41] K.P. Wang, H. Teng, Phys. Chem. Chem. Phys. 11 (2009) 9489–9496.
[42] Y.C. Chen, Y.C. Chang, C.M. Chen, J. Electrochem. Soc. 165 (2018) F409–F416.
[43] J.L. Lan, T.C. Wei, S.P. Feng, C.C. Wan, G. Cao, J. Phys. Chem. C 116 (2012) 25727–25733.
[44] Y. Bai, Q. Yu, N. Cai, et al., Chem. Commun. (Camb.) 47 (2011) 4376–4378.
[45] S. Hattori, Y. Wada, S. Yanagida, S. Fukuzumi, J. Am. Chem. Soc. 127 (2005) 9648–9654.
[46] Y. Cao, Y. Liu, S.M. Zakeeruddin, A. Hagfeldt, M. Grätzel, Joule 2 (2018) 1108–1117.
[47] S. Venkatesan, I.P. Liu, W.N. Hung, H. Teng, Y.L. Lee, Chem. Eng. J. 367 (2019) 17–24.
[48] H.S. Kim, C.R. Lee, J.H. Im, et al., Sci. Rep. 2 (2012) 591.
[49] P. Schulz, D. Cahen, A. Kahn, Chem. Rev. 119 (2019) 3349–3417.
[50] F. Di Giacomo, V. Zardetto, G. Lucarelli, et al., Nano Energy 30 (2016) 460–469.
[51] G. Lucarelli, F. Di Giacomo, V. Zardetto, M. Creatore, T.M. Brown, Nano Res. 10 (2017) 2130–2145.
[52] J. Dagar, S. Castro-Hermosa, G. Lucarelli, F. Cacialli, T.M. Brown, Nano Energy 49 (2018) 290–299.
[53] R. Cheng, C.C. Chung, H. Zhang, et al., Small 15 (2019) e1804465.
[54] H.K.H. Lee, J. Barbé, S.M.P. Meroni, et al., Sol. RRL 3 (2019) 1800207.
[55] C.Y. Chen, J.H. Chang, K.M. Chiang, et al., Adv. Funct. Mater. 25 (2015) 7064–7070.
[56] C.Y. Chen, W.H. Lee, S.Y. Hsiao, et al., J. Mater. Chem. A: Mater. Energy Sustain. 7 (2019) 3612–3617.
[57] M. Li, C. Zhao, Z.K. Wang, et al., Adv. Energy Mater. 8 (2018) 1801509.
[58] L. Lu, T. Zheng, Q. Wu, et al., Chem. Rev. 115 (2015) 12666–12731.
[59] Y. Cai, L. Huo, Y. Sun, Adv. Mater. 29 (2017) 1605437.
[60] L. Sun, X. Xu, S. Song, et al., Macromol. Rapid Comm. 40 (2019) 1900074.
[61] F. Liu, T. Hou, X. Xu, et al., Macromol. Rapid Comm. 39 (2018) 1700555.
[62] S. Park, S.W. Heo, W. Lee, et al., Nature 561 (2018) 516–521.
[63] S.S. Yang, Z.C. Hsieh, M.L. Keshtov, G.D. Sharma, F.C. Chen, Sol. RRL 1 (2017) 1700174.
[64] S. Mori, T. Gotanda, Y. Nakano, et al., J. Appl. Phys. 54 (2015) 071602.
[65] H.K.H. Lee, Z. Li, J.R. Durrant, W.C. Tsoi, Appl. Phys. Lett. 108 (2016) 253301.
[66] Y.J. You, C.E. Song, Q.V. Hoang, et al., Adv. Funct. Mater. (2019) 1901171.
[67] S.C. Shin, C.W. Koh, P. Vincent, et al., Nano Energy 58 (2019) 466–475.
[68] H. Yin, J.K.W. Ho, S.H. Cheung, et al., J. Mater. Chem. A: Mater. Energy Sustain. 6 (2018) 8579–8585.
[69] S.C. Shin, P. Vincent, J.H. Bae, et al., Dyes Pigm. 163 (2019) 48–54.
[70] M. Nam, H.Y. Noh, J. Cho, et al., Adv. Funct. Mater. 29 (2019) 1900154.
[71] C.H. Chen, H.C. Ting, Y.Z. Li, et al., ACS Appl. Mater. Interfaces 11 (2019) 8337–8349.
[72] H.K.H. Lee, J. Wu, J. Barbé, et al., J. Mater. Chem. A: Mater. Energy Sustain. 6 (2018) 5618–5626.
[73] H. Yin, S. Chen, S.H. Cheung, et al., J. Mater. Chem. C Mater. Opt. Electron. Devices 6 (2018) 9111–9118.
[74] A.K. Kyaw, D.H. Wang, V. Gupta, et al., ACS Nano 7 (2013) 4569–4577.
[75] P. Vincent, S.C. Shin, J.S. Goo, et al., Dyes Pigm. 159 (2018) 306–313.
[76] J.S. Goo, J.H. Lee, S.C. Shin, J.S. Park, J.W. Shim, J. Mater. Chem. A: Mater. Energy Sustain. 6 (2018) 23464–23472.
[77] B.R. Lee, J.S. Goo, Y.W. Kim, et al., J. Power Sources 417 (2019) 61–69.
[78] Y. Aoki, Org. Electron. 48 (2017) 194–197.
[79] R. Arai, S. Furukawa, Y. Hidaka, H. Komiyama, T. Yasuda, ACS Appl. Mater. Interfaces 11 (2019) 9259–9264.
[80] B.P. Lechêne, M. Cowell, A. Pierre, et al., Nano Energy 26 (2016) 631–640.
[81] N.F. Yan, G.R. Li, X.P. Gao, J. Mater. Chem. A: Mater. Energy Sustain. 1 (2013) 7012–7015.
[82] B. Lei, G.R. Li, P. Chen, X.P. Gao, Nano Energy 38 (2017) 257–262.